Faraday Discussions
Cite this: DOI: 10.1039/d5fd00064e

PAPER

Self-assembled poly(L-lactide)-based platelets prepared *via* seeded growth†

Laihui Xiao, Tianlai Xia and Rachel K. O'Reilly *

Received 30th April 2025, Accepted 13th May 2025
DOI: 10.1039/d5fd00064e

Crystallization-driven self-assembly (CDSA) offers a powerful approach for constructing well-defined nanostructures; however, achieving precise control over two-dimensional (2D) platelet formation remains challenging, particularly for poly(L-lactide) (PLLA). In this work, we developed a seeded growth strategy using a mixture of homopolymers and diblock polymers to prepare PLLA platelets. In this system, homopolymers facilitate the formation of 2D platelets and enhance crystallization kinetics, while diblock polymers stabilize the platelets and provide functional moieties through their corona-forming block. By systematically optimizing temperature, polymer composition, and polymer length, we achieved size-controllable platelets. Furthermore, we successfully transferred the platelet preparation from batch to a continuous flow system to enable scalable production. This study contributes to the advancement of biodegradable and biocompatible nanoparticles, offering new possibilities for their application in biomedical and functional materials.

1 Introduction

Crystallization can drive the self-assembly of block polymers with a semicrystalline block, which is called crystallization-driven self-assembly (CDSA).[1–3] Since crystallization favors structures of low curvature, anisotropic particles can be obtained in an easier manner by CDSA when compared to common solvent-switching self-assembly of amorphous polymers.[1] Direct CDSA conducted by thermo-control, which involves heating semicrystalline block polymers in a selective solvent to prepare the unimer and then cooling and aging to form self-assembled nanostructures, would lead to polydisperse nanoparticles as nucleation and epitaxial growth occur simultaneously.[4–6] Thus, living CDSA was developed to separate the two processes. This method involves first preparing uniform seed particles, followed by controlled epitaxial growth through either the addition of unimers (polymers dissolved in a good solvent) or annealing to

School of Chemistry, University of Birmingham, Edgbaston, Birmingham B15 2TT, UK. E-mail: r.oreilly@bham.ac.uk

† Electronic supplementary information (ESI) available. See DOI: https://doi.org/10.1039/d5fd00064e

dissolve unstable seeds. In this manner, the size and uniformity of obtained nanostructures can be well controlled.[7–10]

Initially demonstrated by the Manners and Winnik groups using polyferrocenyldimethylsilane (PFS) block polymers,[11,12] CDSA research has expanded to include a broader range of semicrystalline polymers, such as conjugated polymers[13–19] and polyesters.[20–28] Given the demonstrated advantages of anisotropic nanoparticles in biomedical applications, recent efforts have focused on utilizing biocompatible and biodegradable polymers—notably polycaprolactone (PCL) and poly(L-lactide) (PLLA)—for CDSA-based nanoparticle fabrication.[4,29–33] For instance, the O'Reilly group successfully prepared PCL cylinders *via* living CDSA in aqueous media, which were then used as building blocks for biocompatible hydrogels capable of encapsulating cells with high viability.[4] Meanwhile, the Stenzel group developed PLLA platelets and investigated their influence on margination behavior in blood circulation.[30] Their findings revealed that anisotropic nanoparticles exhibited prolonged circulation times and preferential tumor accumulation, highlighting their potential advantages for drug delivery applications.

Although PLLA offers faster degradation and greater mechanical and thermal stability than PCL, its rapid crystallization kinetics and inherent stereostructure make self-assembly, particularly for 2D platelets, more challenging to control.[26,27] Most PLLA platelets with defined dimensions have been prepared *via* self-seeding and by incorporating only diblock polymers to slow down crystallization; however, precise size control remains difficult, as platelet size does not exhibit a linear correlation with parameters such as annealing time or temperature.[34,35] In addition, relying solely on diblock polymers for self-assembly necessitates long aging times due to steric hindrance from the corona-forming block.[35] To date, the only reported living seeded growth approach for PLLA platelets was developed by the Manners group, utilizing a homopolymer with a charged end group as the building block.[36] However, the limited availability of functionalization sites in this polymer constrains the potential applications of the resulting platelets. Thus, achieving precise size-controlled, functionally enhanced PLLA platelets remains a significant challenge.

In this work, we investigated conditions for seeded growth CDSA using a mixture of PLLA homopolymers and diblock polymers as the unimer, a strategy validated in PFS and PCL CDSA systems.[7,9,12,37] In this approach, homopolymers facilitate the formation of 2D structures and enhance crystallization kinetics, while diblock polymers stabilize the platelets and allow functional moieties to be anchored on the corona block. We systematically explored the effects of temperature, unimer composition, and polymer length to achieve precise control over seeded growth. Size-defined platelets were obtained by adjusting the unimer-to-seed ratio. In addition, this strategy was successfully transferred to a continuous flow system, allowing scalable and reproducible platelet production. These findings provide valuable insights into the precise control of platelet morphology and size, which is essential for tailoring materials with specific properties in CDSA applications.

2 Experimental methods

2.1 Materials

L-Lactide was purchased from Corbion-Purac, recrystallized once from dichloromethane and twice from toluene, and subsequently transferred to the glovebox. 1,8-Diazabicyclo[5.4.0]undec-7-ene (DBU) was distilled over CaH_2 and then stored in the glovebox. The dual-functional chain transfer agent (CTA), 2-cyano-5-hydroxypentan-2-yl-ethyl carbonotrithioate (CHPET) was prepared according to our previous work.[4,38] 2,2′-Azobis(2-methylpropionitrile) (AIBN, ≥98%, Sigma Aldrich) was recrystallized in methanol and stored at 4 °C in the dark before use. 1,4-Dioxane (anhydrous, ≥99.8%, Fisher Scientific) and 2-(dimethylamino)ethyl methacrylate (DMAEMA, ≥98%, Sigma Aldrich, contains 700–1000 ppm monomethyl ether hydroquinone as inhibitor) were purified using basic alumina every time before use. Ethanol (anhydrous, ≥99.5%, Fisher Scientific), diethyl ether (anhydrous, ≥99.0%, Fisher Scientific), and chloroform ($CHCl_3$, anhydrous, ≥99%, Sigma Aldrich) were used as received.

2.2 Instrumentation

Nuclear magnetic resonance (NMR), using deuterated chloroform ($CDCl_3$) as the solvent, was performed using a Bruker DPX-400 (400 MHz) spectrometer. MestReNova x64 software was employed for spectra analysis. Size-exclusion chromatography (SEC) was conducted using an Agilent 390-MDS system coupled with PLgel Mixed-D type columns, and signals were detected by refractive index (RI) detector. Elution was performed using chloroform with 0.5% NEt_3, and the flow rate was set at 1 mL min^{-1}. Calibration against polymethyl methacrylate (PMMA) standards using Agilent SEC software was employed to determine number-average (M_n) and weight-average (M_w) molecular weights as well as dispersity ($Đ_M$). Dynamic light scattering (DLS) was performed at 20 °C using a Malvern Zetasizer Nano ZS with a 4 mW He–Ne 633 nm laser module. Measurements were carried out at an angle of 173° (back scattering), and Malvern DTS v7.03 software was used to determine results, such as hydrodynamic diameters (D_h) and size dispersity. D_h values were calculated using the Stokes–Einstein equation where particles are assumed to be spherical. *Z*-Average was taken as the value for size, and reported size distribution was based on scattering intensity. Transmission electron microscopy (TEM) images were captured on a Jeol 1400 Bio TEM microscope with an acceleration voltage of 80 kV. Samples were prepared by drop cast 8 μL of solution on formvar-coated copper grids and then blotting away with filter paper. Then another 8 μL of UA-Zero® EM Stain was dropped on the grid for staining, and the excess was removed by filter paper. Samples were thoroughly dried before testing. Using ImageJ software, at least 100 particles were analyzed to calculate the average size. The number average area (A_n) and weight average area (A_w) were calculated according to eqn (1) and (2), and the uniformity was indicated using distribution determined by A_w/A_n.

$$A_n = \frac{\sum_{i=1}^{n} N_i A_i}{\sum_{i=1}^{n} N_i} \quad (1)$$

$$A_w = \frac{\sum_{i=1}^{n} N_i A_i^2}{\sum_{i=1}^{n} N_i A_i} \quad (2)$$

2.3 Polymerization

2.3.1 Poly(L-lactide) (PLLA). PLLA was prepared by ring-opening polymerization (ROP).[6] In the glovebox filled with N_2, L-lactide (1.65 g, 14.46 mmol), DBU (59.9 μL, 0.4 mmol), CHPET (80 mg, 0.32 mmol), and dichloromethane (15.53 mL) were charged into a 20-mL vial. The mixture was stirred at room temperature for 2 minutes. The product was purified by precipitation once in hexane and twice in methanol. After being dried *in vacuo*, 1.6 g of a yellow solid was obtained.

^{1}H NMR of $PLLA_{45}$ (400 MHz, chloroform-d, δ (ppm)): 5.27–5.05 (m, 90H), 3.35 (q, $J = 7.5$ Hz, 2H), 1.87 (d, $J = 1.4$ Hz, 3H), 1.65–1.45 (m, 270H).

SEC of $PLLA_{45}$ (chloroform, PMMA standard): $M_n = 6.2$ kg mol^{-1}, $Đ_M = 1.30$.

^{1}H NMR of $PLLA_{12}$ (400 MHz, chloroform-d, δ (ppm)): 5.27–5.05 (m, 24H), 3.35 (q, $J = 7.5$ Hz, 2H), 1.87 (d, $J = 1.4$ Hz, 3H), 1.65–1.45 (m, 72H).

SEC of $PLLA_{12}$ (chloroform, PMMA standard): $M_n = 2.8$ kg mol^{-1}, $Đ_M = 1.07$.

2.3.2 Poly(L-lactide)-*b*-poly(2-(dimethylamino)ethyl methacrylate) (PLLA-*b*-PDMAEMA). Reversible addition–fragmentation chain transfer (RAFT) polymerization was conducted to prepare diblock polymer. $PLLA_{45}$ (100 mg, 0.019 mmol), DMAEMA (1.05 g, 6.69 mmol), AIBN (0.61 mg, 0.0037 mmol, 10 mg mL^{-1} in dioxane), and dioxane (2 mL) were charged into an ampoule. The solution underwent three freeze–pump–thaw cycles before being placed in an oil bath at 70 °C. After 7.5 hours, polymerization was terminated by rapidly cooling the ampoule in liquid nitrogen. Once returned to room temperature, the crude product was precipitated three times in cold diethyl ether and collected by centrifugation. After complete drying in a vacuum oven, 622 mg of solid was obtained.

^{1}H NMR of $PLLA_{45}$-*b*-$PDMAEMA_{183}$ (400 MHz, chloroform-d, δ (ppm)): 5.16 (q, $J = 7.1$ Hz, 90H), 4.15–3.97 (m, 366H), 2.64–2.50 (m, 366H), 2.28 (s, 1098H), 1.98–1.78 (m, 366H), 1.61–1.54 (m, 270H), 1.12–0.82 (m, 549H).

SEC of $PLLA_{45}$-*b*-$PDMAEMA_{183}$ (chloroform, PMMA standard): $M_n = 39.3$ kg mol^{-1}, $Đ_M = 1.39$.

2.4 General process of crystallization-driven self-assembly

2.4.1 Seeds prepared by flash-freezing. Seed particles were prepared by a flash-freezing strategy. Specifically, 20 μL of $PLLA_{45}$-*b*-$DMAEMA_{183}$ unimer solution (10 mg mL^{-1} in $CHCl_3$) was added to 2 mL of ethanol, yielding a final polymer concentration of 0.1 mg mL^{-1}. The mixture was heated to 75 °C for 5 minutes to ensure complete dissolution of the polymer, followed by rapid cooling in a dry ice–acetone bath for 1 minute to induce nucleation. The resulting seed particles were then allowed to equilibrate to room temperature before further use.

2.4.2 Living seeded growth in batch. Batch seeded growth was conducted at 500 μL scale, where 50 μL flash-frozen seeds (0.1 mg mL^{-1} in ethanol) were added to 450 μL ethanol. The solution was preheated at various temperatures for 2 min. Then, unimer solution (10 mg mL^{-1} in $CHCl_3$, mixture of homo and diblock polymers) was added, and platelets were obtained after another 2 minute aging.

2.4.3 Living seeded growth in flow. The flow reactor was adapted from our previous work.[38] Seed solution (0.01 mg mL^{-1} in ethanol) was introduced into the reactor by a syringe pump at 200 μL min^{-1} and passed through a preheating channel (200 μL, inner diameter: 0.75 mm) maintained at 50 °C. The seed stream was then combined with unimer solution ($PLLA_{12}$/$PLLA_{45}$-*b*-$PDMAEMA_{183}$ = 1 : 1 wt%, 10 mg mL^{-1} in $CHCl_3$) in a reverse T micromixer. The unimer was delivered by a second syringe pump at flow rates of 2, 4, or 6 μL min^{-1}, corresponding to unimer-to-seed ratios of 10, 20, and 30, respectively. The mixture aged in two downstream channels (inner diameter: 0.3 mm): 100 μL at 50 °C and 300 μL at room temperature (20 °C), before collection.

3 Results and discussion

3.1 Polymer synthesis

Polymers were synthesized according to Scheme 1. PLLA homopolymers ($PLLA_{12}$ and $PLLA_{45}$) were synthesized *via* ROP using CHPET as the initiator and DBU as the catalyst. Chain extension was then performed *via* RAFT polymerization to obtain $PLLA_{45}$-*b*-$PDMAEMA_{183}$ diblock polymer. Polymerization degree was determined by ^1H NMR spectroscopy, while M_n, M_w, and $Đ_M$ were analyzed by SEC. Detailed polymer data are provided in Table S1 and Fig. S1–S4.†

3.2 Seed preparation

In previous CDSA studies, seed particles were typically prepared by sonicating polydisperse cylinders formed through direct CDSA, which involved heating, cooling, and aging steps.[7,39] While effective, this method required several days to a week due to its low efficiency. Recently, our group developed a rapid flash-freezing strategy for seed preparation (Fig. 1a), where the diblock polymer solution is quickly transitioned from undersaturation to supersaturation, inducing uniform self-nucleation within minutes.[40] This approach yielded uniform seed particles within 6 minutes (Fig. 1b), with a measured size of 181 nm by DLS (Fig. 1c), offering a clear improvement over the less regular seeds generated by conventional sonication methods.[36] After that, various conditions were optimized to investigate the epitaxial growth of these seed particles (Scheme 2).

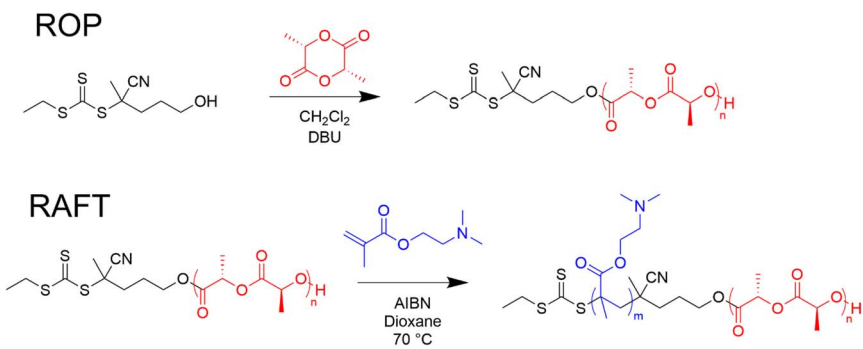

Scheme 1 Synthesis of PLA homopolymer and diblock polymer by ROP and RAFT.

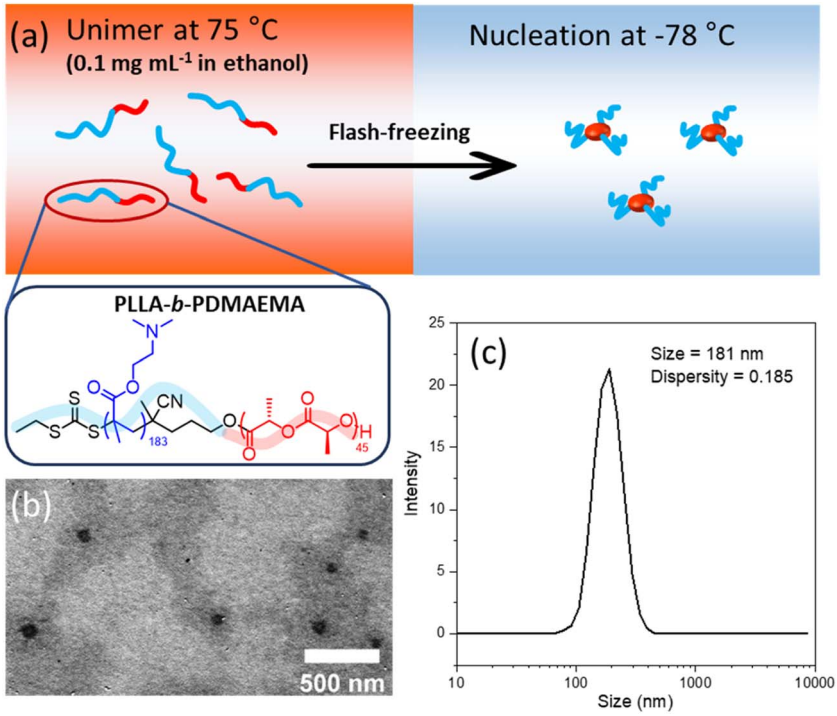

Fig. 1 Seeds prepared by flash-freezing strategy: (a) scheme of seed preparation, (b) TEM image of seeds, and (c) DLS size distribution of seeds. TEM samples were stained. Scale bar = 500 nm.

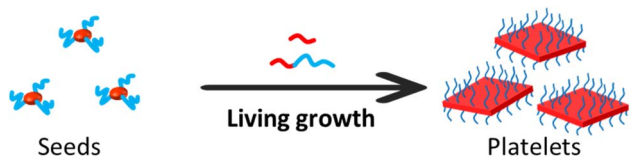

Scheme 2 Schematic illustration of the living CDSA process.

3.3 Effect of temperature

Temperature critically influences crystallization by governing the degree of supercooling (the extent to which the crystallization temperature is below the equilibrium melting temperature), which in turn drives nucleation and growth kinetics.[41–43] To investigate this, living CDSA was conducted using $PLLA_{45}$/$PLLA_{45}$-*b*-$PDMAEMA_{183}$ (1/1 wt%, 10 mg mL^{-1} in $CHCl_3$) at a fixed unimer-to-seed ratio of 10, but at different temperatures, resulting in distinct platelet morphologies (Fig. 2).

At 20 °C (room temperature), the high supercooling degree accelerated both self-nucleation and crystallization kinetics, leading to uncontrolled self-nucleation and the formation of large aggregates rather than uniform epitaxial growth on seed particles (Fig. S5†). As a result, the morphology resembled that of

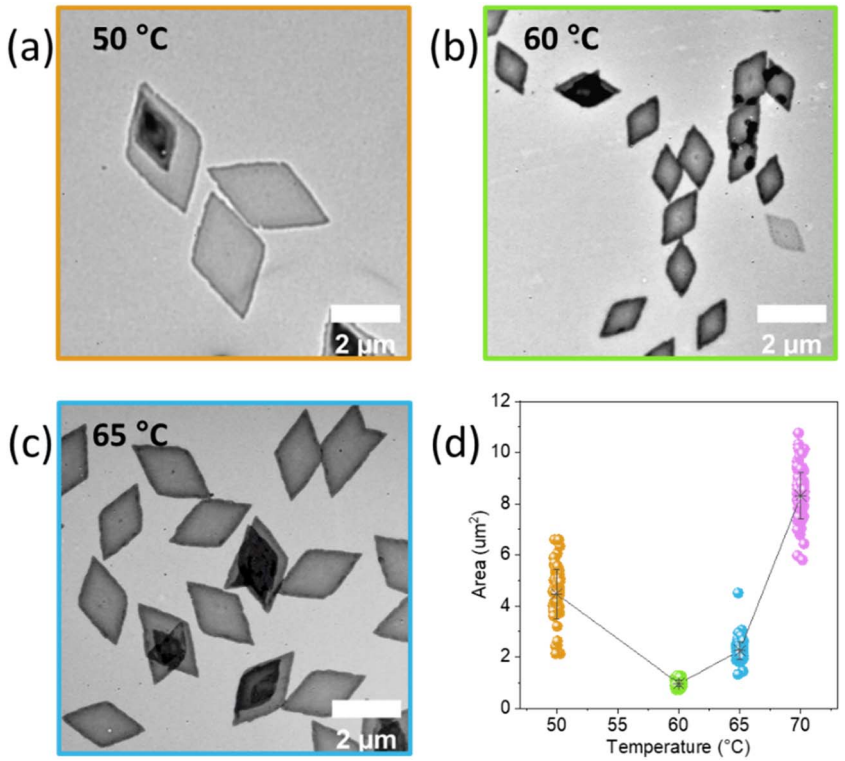

Fig. 2 Platelets prepared at different temperatures: (a), (b), and (c) are TEM images of platelets prepared at 50, 60, and 65 °C, and (d) area variation upon temperature. Scale bar = 2 μm. Platelet size was analyzed from at least 100 particles.

samples prepared without seed particles (Fig. S6†), indicating a loss of seeded growth control.[36] Inspired by previous CDSA studies demonstrating that higher temperatures reduce supercooling and enhance control over seeded growth, we systematically increased the temperature.[38] At 40 °C, self-nucleation remained significant (Fig. S7†), while at 50 °C, well-defined diamond-shaped platelets formed despite residual self-nucleation (Fig. 2a). Increasing the temperature to 60 °C further reduced self-nucleation, yielding more uniform platelets, though unexpectedly, they were smaller than those at 50 °C (Fig. 2b). The high degree of uniformity observed at 60 °C indicates a more controlled and selective seeded growth process, likely due to suppression of competing nucleation pathways. This contrasts with self-seeding behavior, where higher annealing temperatures typically dissolve more seeds, resulting in larger platelets upon regrowth.[40,44] We hypothesize that at 50 °C, seeded growth and self-nucleation occurred at similar rates, leading to partial utilization of active seeds,[45,46] whereas at 60 °C, self-nucleation was suppressed, directing growth more effectively onto available seeds and yielding smaller, more uniform platelets. As the temperature further increased to 65 and 70 °C (Fig. 2c and S8†), platelet size continued to increase (Fig. 2d and Table S2†), aligning with reported studies.[47–49] These findings demonstrate that temperature regulation is a key strategy for controlling seeded

growth. However, self-nucleation persisted in all samples, likely due to insufficient steric stabilization from the low corona density of the diblock polymer, which may have permitted secondary nucleation.[50]

3.4 Effect of unimer composition

To further enhance the control over seeded growth, we adjusted the unimer composition by increasing the proportion of diblock polymer while reducing the homopolymer content. Since homopolymers promote rapid epitaxial growth, decreasing their fraction was expected to slow the growth rate and improve uniformity.[51] As anticipated, platelet uniformity was significantly enhanced, and self-nucleation was effectively suppressed when the homopolymer-to-diblock polymer ratio was reduced to 1/2 (Fig. 3a). This improvement was attributed to the increased corona density on platelet surfaces, which provided greater steric hindrance and prevented secondary nucleation. A similar trend was observed when the diblock polymer fraction was further increased (Fig. 3b and c).

Interestingly, despite maintaining a constant unimer-to-seed ratio of 10, platelet size decreased with higher diblock polymer content (Fig. 3d and Table

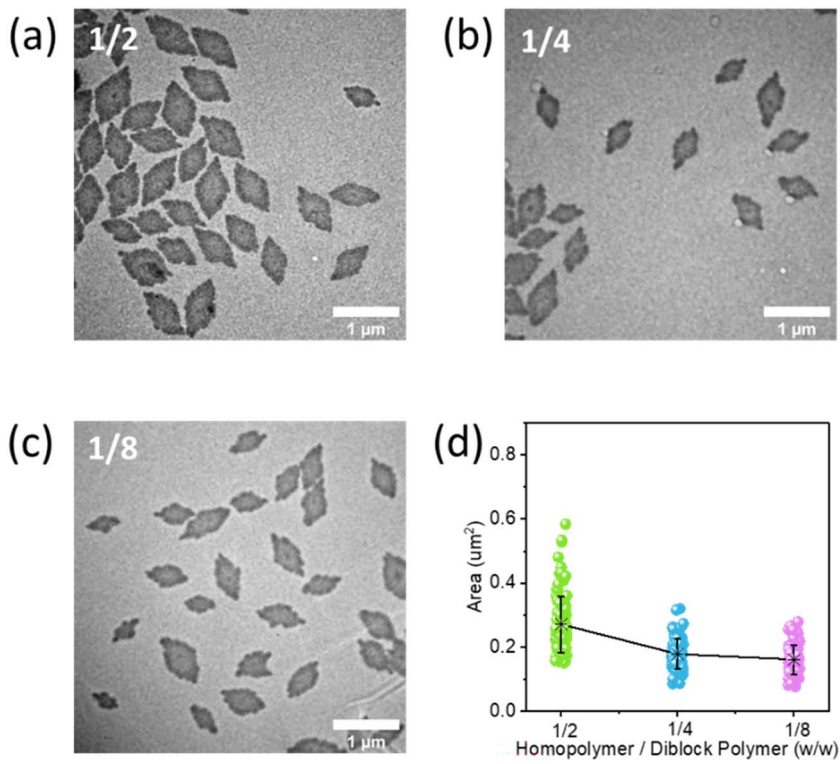

Fig. 3 Platelets prepared using unimer of various $PLLA_{45}/PLLA_{45}$-*b*-$PDMAEMA_{183}$ ratios at the fixed unimer-to-seed ratio of 10: (a), (b), and (c) are TEM images of platelets prepared using unimer with the $PLLA_{45}/PLLA_{45}$-*b*-$PDMAEMA_{183}$ mass ratios of 1/2, 1/4, and 1/8, respectively, and (d) area variation upon $PLLA_{45}/PLLA_{45}$-*b*-$PDMAEMA_{183}$ ratios. Scale bar = 1 μm. Platelet size was analyzed from at least 100 particles.

S2†). This was attributed to the reduced PLLA fraction, which directly forms the crystalline platelet core. Moreover, increasing the diblock polymer fraction altered the morphology of the nanoparticles, causing the initially distinct diamond-shaped features to become less pronounced and more ambiguous. This change in shape was accompanied by a reduction in uniformity (the A_w/A_n values remained elevated between 1.07–1.10, Table S2†), suggesting that the higher density of corona chains not only restricts lateral growth but also introduces inconsistencies during crystallization. As the corona density increases, steric repulsion between the corona blocks can hinder lateral crystal growth at the edges, especially along the shorter axis, resulting in more anisotropic or ill-defined structures.[52,53] A similar transition from 2D platelets to 1D cylinders has been reported when using only diblock polymer as the unimer for seeded growth.[4,6] These observations highlight the crucial role of homopolymer content in stabilizing the 2D morphology.

3.5 Effect of homopolymer molecular weight

To balance the need for well-defined platelet formation with controlled seeded growth, short-chain homopolymer was used as a compromise strategy. This approach was based on previous findings that polymer crystallization ability increases with molecular weight.[39] As anticipated, uniform platelets with well-defined morphology were obtained when unimer solution was added at a unimer-to-seed ratio of 10 (Fig. 4a). Notably, no significant self-nucleation was observed, which may be attributed to the short homopolymer reducing chain folding during crystallization, thereby minimizing lattice imperfections that could otherwise promote secondary nucleation.[54]

To further investigate the living behavior of epitaxial growth, additional aliquots of unimer solution were introduced sequentially. The platelet size increased proportionally with unimer addition (Fig. 4b and c), and statistical analysis confirmed a linear relationship between platelet size and unimer-to-seed ratio (Fig. 4d and Table S2†). This result not only validated the living nature of the growth process but also provided a foundation for precise platelet size control. Moreover, it highlighted the dominant role of homopolymer in seeded growth using mixed unimers, establishing a basis for the further development of functional PLLA-based platelets.

3.6 Seeded growth in the flow reactor

To improve the scalability of platelet preparation, seeded growth was transferred from batch to a continuous flow system (Fig. 5a). In this setup, the seed stream was preheated to 50 °C to enhance mixing efficiency upon merging with the unimer stream, as elevated temperatures in flow are known to improve mixing and promote uniform particle formation.[38] Aging initially occurred at 50 °C to ensure thorough mixing, followed by further aging at room temperature in a downstream channel before collection. Using a unimer-to-seed ratio of 10, uniform platelets ($A_n = 0.39\ \mu m^2$, $A_w/A_n = 1.08$, Fig. 5b) were obtained, closely matching those from batch synthesis ($A_n = 0.44\ \mu m^2$, $A_w/A_n = 1.05$, Fig. 4a). By varying the flow rate of unimer, higher unimer-to-seed ratios (20 and 30) were achieved, producing platelets with corresponding increases in area (Fig. 5c and d), which followed the same linear trend observed in batch (Fig. 5e). Thus, the

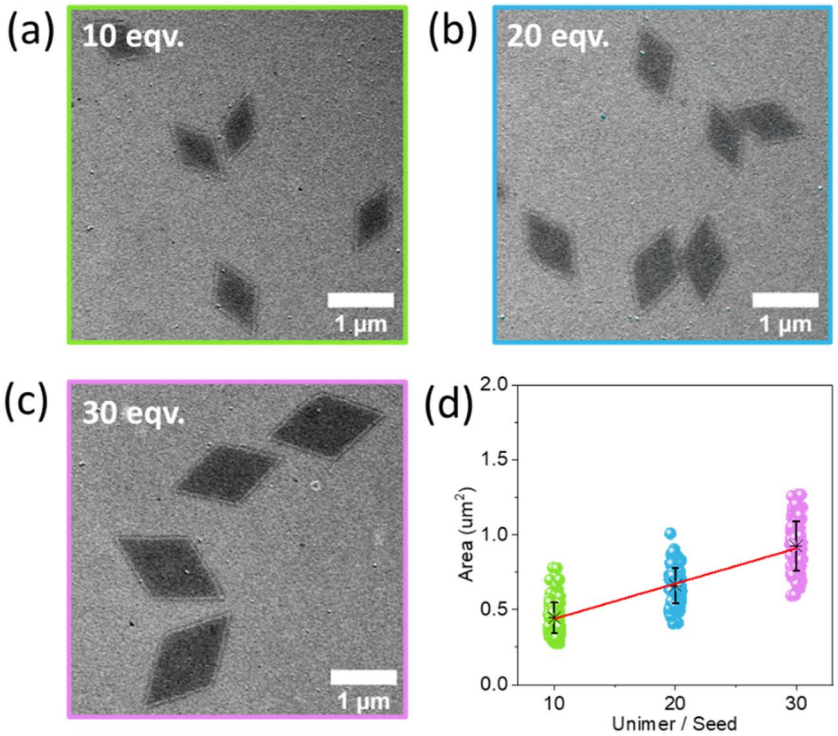

Fig. 4 Size-controllable platelets prepared by living CDSA using $PLLA_{12}/PLLA_{45}$-*b*-$PDMAEMA_{183}$ at mass ratio of 1/1: (a), (b), and (c) are TEM images of platelets prepared at various unimer-to-seed ratios, and (d) linear fit of area upon different unimer-to-seed ratios. Scale bar = 1 μm. Platelet size was analyzed from at least 100 particles.

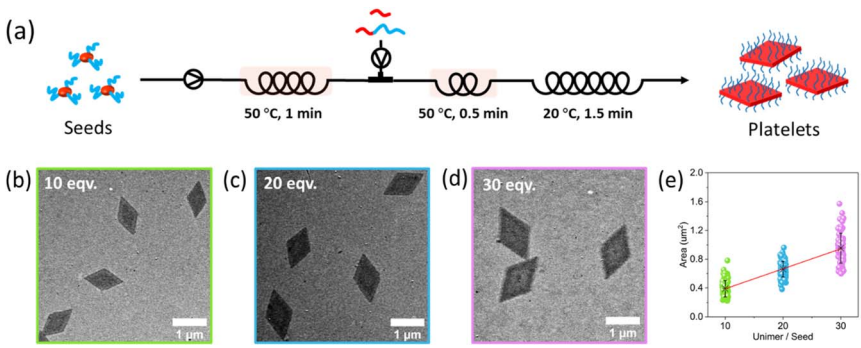

Fig. 5 Flow living CDSA preparing size-controllable platelets using $PLLA_{12}/PLLA_{45}$-*b*-$PDMAEMA_{183}$: (a) scheme of preparing platelets in the flow reactor, (b), (c) and (d) are TEM images of platelets prepared at various unimer-to-seed ratios, and (e) linear fit of area upon different unimer-to-seed ratios. Scale bar = 1 μm. Platelet size was analyzed from at least 100 particles.

successful transfer of seeded growth from batch to flow demonstrated that uniform platelets could be reproducibly prepared under continuous conditions, with control comparable to that in batch systems. This approach lays a solid foundation for future large-scale manufacturing and broadens the potential for practical applications of these nanostructures in areas such as drug delivery, sensing, and nanofabrication.

4 Conclusion

In this study, we investigated the effects of temperature, unimer composition, and homopolymer length on the controlled seeded growth of CDSA using a mixed unimer system composed of PLLA homopolymers and diblock polymers. Our results showed that temperature played a significant role in seeded growth. Higher temperatures reduced the growth rate by decreasing the degree of supercooling, resulting in platelets of uniform size, even though surface nucleation could still occur. Increasing the proportion of diblock polymers in the unimer suppressed surface nucleation but led to platelets with ambiguous shapes, indicating that a sufficient amount of homopolymer was necessary to form well-defined platelet morphologies. To address this, we maintained the original homopolymer content (50 wt%) while shortening its length, which reduced the crystallization rate and allowed for the formation of well-defined diamond-shaped platelets. By adjusting the amount of unimer added to the seed solution, we could further control platelet size. Additionally, this methodology was successfully transferred to a continuous flow system, enabling scalable production of size-controlled platelets. This work not only provides fundamental insights into the role of polymer composition in CDSA but also lays the groundwork for designing functional, biodegradable platelet-based materials for biomedical and nanotechnological applications.

Data availability

Supporting material, including text, figures, and tables are available in the ESI.†

Author contributions

ROR and LX conceived the work. LX, TX and ROR designed the experiments. LX and TX performed the experiments. All authors contributed to the analysis of the data. ROR directed the research. LX and ROR prepared the manuscript, and all authors contributed to manuscript revisions.

Conflicts of interest

There are no conflicts to declare.

Acknowledgements

The authors would like to thank the University of Birmingham and China Scholarship Council for funding and support.

References

1 L. MacFarlane, C. Zhao, J. Cai, H. Qiu and I. Manners, *Chem. Sci.*, 2021, **12**, 4661–4682.
2 S. Ganda and M. H. Stenzel, *Prog. Polym. Sci.*, 2020, **101**, 101195.
3 A. K. Pearce, T. R. Wilks, M. C. Arno and R. K. O'Reilly, *Nat. Rev. Chem.*, 2020, **5**, 21–45.
4 M. C. Arno, M. Inam, Z. Coe, G. Cambridge, L. J. Macdougall, R. Keogh, A. P. Dove and R. K. O'Reilly, *J. Am. Chem. Soc.*, 2017, **139**, 16980–16985.
5 G. Guérin, H. Wang, I. Manners and M. A. Winnik, *J. Am. Chem. Soc.*, 2008, **130**, 14763–14771.
6 Y. He, J.-C. Eloi, R. L. Harniman, R. M. Richardson, G. R. Whittell, R. T. Mathers, A. P. Dove, R. K. O'Reilly and I. Manners, *J. Am. Chem. Soc.*, 2019, **141**, 19088–19098.
7 T. Xia, Z. Tong, Y. Xie, M. C. Arno, S. Lei, L. Xiao, J. Y. Rho, C. T. J. Ferguson, I. Manners, A. P. Dove and R. K. O'Reilly, *J. Am. Chem. Soc.*, 2023, **145**, 25274–25282.
8 Z. Tong, Y. Xie, M. C. Arno, Y. Zhang, I. Manners, R. K. O'Reilly and A. P. Dove, *Nat. Chem.*, 2023, **15**, 824–831.
9 Y. Xie, Z. Tong, T. Xia, J. C. Worch, J. Y. Rho, A. P. Dove and R. K. O'Reilly, *Adv. Mater.*, 2024, **36**, 2308154.
10 L. Liu, C. T. J. Ferguson, L. Zhu, S. Chen, R.-Y. Wang, S. Wang, A. P. Dove, R. K. O'Reilly and Z. Tong, *Nat. Synth.*, 2024, **3**, 903–912.
11 X. Wang, G. Guerin, H. Wang, Y. Wang, I. Manners and M. A. Winnik, *Science*, 2007, **317**, 644–647.
12 H. Qiu, Y. Gao, C. E. Boott, O. E. C. Gould, R. L. Harniman, M. J. Miles, S. E. D. Webb, M. A. Winnik and I. Manners, *Science*, 2016, **352**, 697–701.
13 B. Xiang, H. Wu, R. Chen, X. Huang, G. Lu and C. Feng, *Polym. Chem.*, 2024, **15**, 4231–4243.
14 M. Vespa, L. R. MacFarlane, Z. M. Hudson and I. Manners, *Polym. Chem.*, 2024, **15**, 1839–1850.
15 S. Park, S.-Y. Kang, S. Yang and T.-L. Choi, *J. Am. Chem. Soc.*, 2024, **146**, 19369–19376.
16 F. Huang, J. Ma, J. Nie, B. Xu, X. Huang, G. Lu, M. A. Winnik and C. Feng, *J. Am. Chem. Soc.*, 2024, **146**, 25137–25150.
17 C. Duan, B. Xu, R. Li, X. Huang, S. Lin and C. Feng, *Sci. China:Chem.*, 2024, **67**, 2341–2352.
18 Y. Zhang, J. Tian, H. Shaikh, H. K. MacKenzie, Y. He, C. Zhao, S. Lei, Y. Ren and I. Manners, *J. Am. Chem. Soc.*, 2023, **145**, 22539–22547.
19 N. Yun, C. Kang, S. Yang, S.-H. Hwang, J.-M. Park and T.-L. Choi, *J. Am. Chem. Soc.*, 2023, **145**, 9029–9038.
20 Z. Gao, X. Zhang, B. Zheng, J. Gu and Z. Tong, *J. Am. Chem. Soc.*, 2025, **147**, 5172–5181.
21 J. Yu, J. Liu, C. Li, J. Huang, Y. Zhu and H. You, *Chem. Commun.*, 2024, **60**, 3217–3225.
22 S. D. Dale, J. Beament, A. P. Dove and R. K. O'Reilly, *RSC Appl. Polym.*, 2024, **2**, 957–963.
23 L. Zhu, B. Xiang, Y. Su and Z. Tong, *Polymer*, 2023, **272**, 125831.

24 X. Zhang, G. Chen, B. Zheng, Z. Wan, L. Liu, L. Zhu, Y. Xie and Z. Tong, *Biomacromolecules*, 2023, **24**, 1032–1041.
25 C. Clamor, S. D. Dale, J. Beament, E. Mould, R. K. O'Reilly and A. P. Dove, *Macromolecules*, 2023, **56**, 9821–9828.
26 Y. Xie, W. Yu, T. Xia, R. K. O'Reilly and A. P. Dove, *Macromolecules*, 2023, **56**, 7689–7697.
27 L. Sun, A. Pitto-Barry, N. Kirby, T. L. Schiller, A. M. Sanchez, M. A. Dyson, J. Sloan, N. R. Wilson, R. K. O'Reilly and A. P. Dove, *Nat. Commun.*, 2014, **5**, 5746.
28 N. Petzetakis, D. Walker, A. P. Dove and R. K. O'Reilly, *Soft Matter*, 2012, **8**, 7408–7414.
29 S. Ganda, C. K. Wong, J. Biazik, R. Raveendran, L. Zhang, F. Chen, N. Ariotti and M. H. Stenzel, *ACS Appl. Mater. Interfaces*, 2022, **14**, 35333–35343.
30 J. T. Lovegrove, R. Raveendran, P. Spicer, S. Förster, C. J. Garvey and M. H. Stenzel, *ACS Macro Lett.*, 2023, **12**, 344–349.
31 S. Ganda, C. K. Wong and M. H. Stenzel, *Macromolecules*, 2021, **54**, 6662–6669.
32 Z. Li, L. Sun, Y. Zhang, A. P. Dove, R. K. O'Reilly and G. Chen, *ACS Macro Lett.*, 2016, **5**, 1059–1064.
33 Z. Li, Y. Zhang, L. Wu, W. Yu, T. R. Wilks, A. P. Dove, H.-m. Ding, R. K. O'Reilly, G. Chen and M. Jiang, *ACS Macro Lett.*, 2019, **8**, 596–602.
34 M. C. Arno, M. Inam, A. C. Weems, Z. Li, A. L. A. Binch, C. I. Platt, S. M. Richardson, J. A. Hoyland, A. P. Dove and R. K. O'Reilly, *Nat. Commun.*, 2020, **11**, 1420.
35 M. Inam, J. R. Jones, M. M. Pérez-Madrigal, M. C. Arno, A. P. Dove and R. K. O'Reilly, *ACS Cent. Sci.*, 2018, **4**, 63–70.
36 X. He, M.-S. Hsiao, C. E. Boott, R. L. Harniman, A. Nazemi, X. Li, M. A. Winnik and I. Manners, *Nat. Mater.*, 2017, **16**, 481–488.
37 R. Tao, H. Wang, R. Hou, B. Zheng, Y. Zhao, Y. Xie and Z. Tong, *Adv. Funct. Mater.*, 2025, **35**, 2500737.
38 L. Xiao, S. J. Parkinson, T. Xia, P. Edge and R. K. O'Reilly, *ACS Macro Lett.*, 2023, **12**, 1636–1641.
39 T. Xia, L. Xiao, K. Sun, J. Y. Rho, Y. Xie, S. J. Parkinson, L. Sangroniz, J. Zhang, J. Lin, A. J. Müller, L. Gao, A. P. Dove and R. K. O'Reilly, *Macromolecules*, 2024, **57**, 11210–11220.
40 L. Xiao, T. Xia, J. Zhang, S. J. Parkinson, J. Y. Rho, A. P. Dove and R. K. O' Reilly, *Nat. Synth.*, 2025, **4**, 808–815.
41 L. Liu, X. Meng, M. Li, Z. Chu and Z. Tong, *ACS Macro Lett.*, 2024, **13**, 542–549.
42 L. Liu, L. Zhu, Z. Chu and Z. Tong, *Macromolecules*, 2023, **56**, 5984–5992.
43 L. Zhu, L. Liu, S. Varlas, R.-Y. Wang, R. K. O'Reilly and Z. Tong, *ACS Nano*, 2023, **17**, 24141–24153.
44 H. Kim, J. Lee, S.-H. Hwang, N. Yun, S. Park and T.-L. Choi, *J. Am. Chem. Soc.*, 2024, **146**, 20750–20757.
45 Y. Song, X. Huang, G. Lu and C. Feng, *Macromolecules*, 2025, **58**, 1023–1037.
46 S. T. G. Street, Y. He, R. L. Harniman, J. D. Garcia-Hernandez and I. Manners, *Polym. Chem.*, 2022, **13**, 3009–3025.
47 C. Wang, F. Huang, X. Huang, G. Lu and C. Feng, *Macromol. Rapid Commun.*, 2024, **45**, 2300482.
48 J. Ma, F. Huang, S. Zhang, J. Ye, X. Huang, G. Lu and C. Feng, *Macromolecules*, 2023, **56**, 8529–8546.

49 W. Yu, J. C. Foster, A. P. Dove and R. K. O'Reilly, *Macromolecules*, 2020, **53**, 1514–1521.
50 J. Jiang, E. Nikbin, Y. Liu, S. Lei, G. Ye, J. Y. Howe, I. Manners and M. A. Winnik, *J. Am. Chem. Soc.*, 2023, **145**, 28096–28110.
51 R. Deng, X. Mao, S. Pearce, J. Tian, Y. Zhang and I. Manners, *J. Am. Chem. Soc.*, 2022, **144**, 19051–19059.
52 G. Rizis, T. G. M. van de Ven and A. Eisenberg, *Angew. Chem., Int. Ed.*, 2014, **53**, 9000–9003.
53 G. Rizis, T. G. M. van de Ven and A. Eisenberg, *ACS Nano*, 2015, **9**, 3627–3640.
54 T. Zhou, H. Qi, L. Han, D. Barbash and C. Y. Li, *Nat. Commun.*, 2016, **7**, 11119.